

Article

The Controlling Effects of Compositions on Nanopore Structure of Over-Mature Shale from the Longtan Formation in the Laochang Area, Eastern Yunnan, China

Xiaoli Zhang ^{1,2}, Caifang Wu ^{1,2,*}, Jinxian He ^{1,2}, Zeqiang Ren ^{1,2} and Taotao Zhou ^{1,2}

¹ Key laboratory of Coalbed Methane Resource and Reservoir Formation Process, Ministry of Education, China University of Mining and Technology, Xuzhou 221116, China

² School of Resources and Geoscience, China University of Mining and Technology, Xuzhou 221116, China

* Correspondence: 4591@cumt.edu.cn

Received: 17 April 2019; Accepted: 27 June 2019; Published: 30 June 2019



Abstract: Over-mature shale has undergone complex geological processes, e.g., diagenesis, deep thermolysis, epigenesis, and metamorphism. During this series of processes, the internal components of shale are transformed coordinatively, and the special pore structure with a complex genesis in the over-mature shale is formed. The study of the special pore structure of over-mature shale and its main controlling factors can provide theoretical support for shale gas exploration and development. In this study, the over-mature shale of the Longtan Formation in the Laochang area, eastern Yunnan Province, China, was tested and analyzed to determine the total organic carbon content, kerogen microscopic composition, and its vitrinite reflectance. Moreover, the mineral composition and pore characteristics of the shale were tested using X-ray diffraction, the argon ion polishing field emission scanning electron microscopy technique, and the low temperature nitrogen adsorption experiment. The results show that the compositions of Longtan Formation shales have a low rigid clastic particles content, high clay content, and abundant metasomatic ankerite, and that the organic matter, dominated by type III, is highly mature. At the same time, the shale pore structure is characterized by a large average pore size, well-developed macropores, and a high number of micropores and mesopores. By analyzing the transformation of the mineral composition of shale during thermal evolution, the controlling factors of pore structure are determined. During the evolution of shale, the intergranular pores (mainly large pores) between rigid minerals are destroyed in large quantities. After a short period, a large number of dissolved pores with the pore size of macropores are formed in the acid-resistant minerals under the action of organic acid. These dissolved pores, together with the remaining intergranular pores of rigid minerals and micro-fractures, form most of the macropores of shale. There is a large amount of ankerite in over-mature shale formed during metasomatism, which occludes some pores of shale. However, intragranular pores and cleavage-sheets develop in ankerite, contributing some porosity to the shale reservoir. Inter-clay pores and organic matter pores constitute most shale micro and mesopores, and between which inter-clay pores take dominance.

Keywords: over-mature shale; nanopore structure; Longtan Formation; field emission scanning electron microscopy; nitrogen adsorption

1. Introduction

Paleozoic shale is thick and widespread in southern China and has good prospects for shale gas exploration and development [1]. Compared to the commercially developed shale gas reservoirs in foreign countries, i.e., Antrim shale [2], Ohio shale [3], Barnett shale [4], Haynesville shale [5], and

Marcellus shale [6], the Paleozoic shale in southern China generally has a high degree of thermal evolution [7,8]. Geological research of conventional oil and gas have suggested that a high degree of thermal evolution reflects a poor hydrocarbon generation potential of the shale. However, research on shale gas reservoir formation shows that high maturity may be beneficial to shale gas [8,9]. In addition, breakthroughs have been made in the black shale of the Lower Cambrian Qiongzhusi Formation and the Upper Ordovician Wufeng Formation-Lower Silurian Longmaxi Formation (at the over-mature stage, vitrinite reflectance (R_o) is greater than 2.0%) in the exploration of shale gas in China in recent years, and high-yield wells with a daily production of hundreds of thousands of cubic meters per day are drilled [10–12]. The development potential of over-mature shale gas resources, especially the microscopic characteristics [13] and gas storage capacity of over-mature shale reservoirs has become an important research direction for promoting shale gas exploration and development in China.

Over-mature shale has undergone a series of geological processes, such as diagenesis, deep thermolysis, epigenesis, and metamorphism. The organic components and inorganic minerals in shale are intensively reformed. The kerogen has a high degree of thermal evolution (R_o is greater than 2.0%) and generally enters a dry gas window. Highly ordered clusters with a large number of pore structures are formed inside kerogen as a result of cracking. At the same time, the vitrinite group exhibits anisotropy [14,15]. Orderly transformation and orientation are characteristics of clay minerals [16], which are dominated by mixed illite/smectite. Almost all smectite and kaolinite convert into illite, and chlorite also appears. Together with the changes in the composition of clay minerals, the pore structure of the clay matrix also adjusts accordingly, including changes in matrix pores and the deformation of clay minerals. Rigid mineral particles undergo diagenesis, such as cementation, dissolution, recrystallization, and metasomatism. The conversion or disappearance of primary minerals and the formation of new minerals has strongly modified the pore structure of shale. There is no doubt that the staged transformation of over-mature thermal evolution has strongly modified the composition and structure of shale. Therefore, how these factors affect shale reservoir properties needs to be further explained.

In this paper, the over-mature shale of the Longtan Formation in the Laochang area of eastern Yunnan Province was tested for its organic matter and mineral composition. The microscopic pore types, sizes, morphology, and structures were analyzed. The controlling effects of the thermal evolution of organic matter and mineral diagenesis on pores in over-mature shale was discussed. By analyzing the transformation of mineral composition in shale during thermal evolution, and the relationship between the composition of over-mature shale and its pore morphology, size, and types of over-mature shale, the controlling factors of the nano-pore structure of over-mature shale were determined.

2. Sample and Experiment

2.1. Geological Background and Samples

Located in Fuyuan County, Yunnan Province, the Laochang area is part of the Liupanshui coalfield. The tectonic setting of the Laochang area belongs to the contact transition zone between the Diandong platform fold belt of the Yangtze paraplatform and the Diandong fold belt of the South China fold system [17–19]. With an average thickness of about 350 m, the Longtan Formation is a set of coal-bearing rock series of transitional facies, which is composed of gray to gray-black fine sandstone, siltstone, shale, carbonaceous shale, and a coal seam. It is characterized by widespread, multiple layers, a large cumulative thickness, and its interbeddedness with a coal seam, and the shale of the Longtan Formation provides a material basis for the development of shale gas. In the Late Permian, there were many phases of basalt eruption and basic magma intrusion in the study area [17]. At the end of the Indosinian tectonic period, the Longtan Formation had a buried depth of more than 4000 m. Under the joint action of deep burial and basic magma, the maturity of the organic matter of the Longtan Formation shale has reached the over-mature stage. In the Himalayan period, the Longtan Formation was uplifted to the shallow part of its present buried depth of less than 1000 m [20].

The 9 over-mature shale samples were collected from the Longtan Formation from wells S1 and S2 in the Laochang area, eastern Yunnan Province.

2.2. Experimental Methods and Instruments

The mineral composition test was carried out with an AXS D8 ADVANCE X-ray diffractometer (Bruker, Billerica, MA, USA), with a Cu target and Ka radiation. The working conditions were a 40 kV voltage and a 30 mA current. The cable slit of the incident side and the diffraction side were both 2.5 degrees. The mass fractions of the different mineral components in the shale samples were calculated in line with the semi-quantitative principle. The scanning speed of the total rock analyses was set to 4°/min and the scanning angle ranged from 3° to 70°.

The method for measuring the total organic carbon (TOC) content was the carbon sulfur measurement method, and the instrument used was an Analytikjena multi EA 4000 elemental analyzer (Analytik Jena AG, Jena, Germany). After the samples were burned at a high temperature, the organic carbon content of the samples was calculated by measuring the peak area of carbon dioxide using the infrared absorption method.

The kerogen type and vitrinite reflectance (Ro) were tested using microscopy. Firstly, an acid and alkali treatment, heavy liquid flotation, and centrifugation was carried out to separate and enrich the kerogen, and then the type and content of the kerogen components were measured and judged using a binocular microscope equipped with an oil immersion objective lens and a photometer in order to further measure the vitrinite reflectance.

A ZEISS SIGMA 500/VP high-resolution field emission scanning electron microscope (Carl Zeiss AG, Jena, Germany) was used in the high vacuum scanning mode, with a minimum resolution of 1.6 nm. The samples were polished by sub-ions using a Gatan 697 Ilion II Datasheet wide beam argon ion polishing system (Gatan, Pleasanton, CA, USA) before being observed. The sample surface was bombarded with a sub-ion beam to obtain a high-quality surface layer.

The low temperature nitrogen adsorption experiment was carried out using a Micromeritic Tristar II3020 fully automatic specific surface area and pore analyzer (Micromeritics Instrument, Norcross, GA, USA). The pore size ranged from 1.2 nm to 200 nm. The lowest measurable specific surface area was 0.0005 m²/g, and the minimum pore volume was 0.1 mm³/g. The samples were pretreated before the experiment. The shale samples were screened using a 60-mesh sieve after being ground, and the samples below 60 meshes were selected. After water and volatiles were removed in a vacuum drying environment, the samples were placed in the instrument for analyses. A low temperature and low-pressure environment was maintained (77.15 K and 127 KPa) during the experiment.

3. Results

3.1. Minerals Composition and Maturity Analysis

The basic characteristics of the samples are shown in Table 1. It can be seen that the organic matter was type III and had a high degree of thermal evolution, with an Ro of greater than 2%, which is over-matured. The clay minerals were at the late diagenetic stage B, since they were dominated by mixed illite/smectite with minor illite and chlorite, and an absence of smectite and kaolinite. In addition to rigid particles, such as quartz and plagioclase, large amounts of metasomatic ankerite and siderite formed the main part of the brittle minerals. Calcite was absent due to intense metasomatism in the late diagenetic stage. Compared with shale from the Longmaxi-Wufeng Formation in South Sichuan [21–25], the Longtan Formation shale has a low rigid particle content, a high clay mineral content, and a high metasomatic carbonate content, as well as type III organic matter, which has a great potential for acid generation during thermal evolution. Compared with shale from Shanxi-Taiyuan [26,27] and the Yanchang Formation [28] in the Ordos basin, the Longtan Formation shale has a high organic matter content and a high maturity. The composition of the shale provides a material basis for the special pore structure.

Table 1. XRD analysis and organic geochemical analysis results of the shale samples from the Laochang area, eastern Yunnan, China.

Sample ID	Depth (m)	Minerals (wt. %)												TOC (%)	Ro (%)	KT	
		Q.	Fs.	Pl.	Cc.	An.	Py.	Si.	Kl.	Ch.	Il.	Mo.	Mixed I/S				I/S Ratio
S1-1	746.8	5	0	19	0	3	0	9	0	2	6	0	56	25	3.0	2.19	III
S1-2	789.2	11	0	6	0	0	0	2	0	2	8	0	70	15	3.5	2.26	III
S1-3	823.7	10	0	12	0	9	0	7	0	2	6	0	54	20	3.4	2.54	III
S2-1	611.7	17	0	8	0	12	0	4	0	2	6	0	51	15	2.6	2.31	III
S2-2	632.0	20	0	8	0	17	0	16	0	1	4	0	34	20	2.4	2.1	III
S2-3	653.6	25	0	12	0	5	4	15	0	1	4	0	34	20	2.9	2.17	III
S2-4	662.0	16	0	13	0	14	0	1	0	2	6	0	49	20	2.6	2.33	III
S2-5	669.6	17	0	11	0	12	3	1	0	2	6	0	49	15	3.5	2.33	III
S2-6	736.5	12	0	14	0	22	2	2	0	1	5	0	42	15	2.0	2.34	III

Note: Q., quartz; Fs., feldspar; Pl., plagioclase; Cc., calcite; An., ankerite; Py., pyrite; Si., siderite; Kl., kaolinite; Ch., Chlorite; Il., illite; Mo., montmorillonite; TOC., total organic carbon; Ro., Vitrinite reflection; KT, kerogen type.

3.2. Pore Types

A total of nine typical over-mature shale samples of the Longtan Formation were selected from two wells in the Laochang area for argon ion polishing. Four types of pore were observed under field emission scanning electron microscopy, including intragranular pores, intergranular pores, organic pores, and microcracks. The pore types of the Longtan Formation shale are characterized by the appearance of dissolved pores and crystal defect pores in ankerite, and the large development of inter-sheet pores between clays and gas pores.

3.2.1. Intergranular Pores

Large amounts of rigid minerals, such as quartz and plagioclase, developed in the Longtan Formation shale in the Laochang area (Table 1). There is a difference in the hardness between rigid minerals and clay minerals, as well as between organic matter. Clay minerals and organic matter deform around rigid minerals under stress, retaining crescent-shaped pores at the edge of the particles (Figure 1a), with an average pore diameter of 500 nm and a general degree of development. In addition, over-mature shale generally develops directional sheet-like and silky clay minerals. These clay minerals overlap each other to form an inter-sheet pore of about 15 nm (Figure 1b), which is widespread in shale. In the local flexural deformation zone, the clay pieces come together to form a triangular lattice, and the inter-sheet pores can increase to 50–80 nm (Figure 1b).

3.2.2. Intragranular Pores

The intragranular pores of the Longtan Formation shale reservoirs include dissolved pores, the intercrystalline pores of pyrite nodules, and crystal defect pores in ankerite. Most dissolved pores occur in the immediate vicinity of organic matters (Figure 1c), reflecting the importance of the thermal evolution and acid discharge of organic matters for the development of such pores. The dissolved pores are irregular in shape, with edges that are harbor-shaped, with an average pore diameter of 2000 nm. Even though not too many developed in the shale, such pores contribute greatly to pore structures. Besides increasing porosity, dissolved pores also enhance pore connectivity. Strawberry-like pyrite tuberculoids developed in the shales of the Longtan Formation. The triangular and rhomboid pyrite intergranular pores (Figure 1d) within the strawberry-like pyrite tuberculoids had an average pore diameter of 50 nm, and were locally developed. Intragranular defect pores within ankerite developed in shale (Figure 1e). Unlike dissolved pores, these intragranular pores are distributed in bands (Figure 1f) and have no positional relationship with organic matter. In addition, these intragranular pores have straight walls (Figure 1e) and occur inside the ankerite with clear and complete grain boundaries.

3.2.3. Organic Matter Pores

Formed in the organic matter during its burial and thermal evolution, organic matter pores include cell pores and gas pores, which are the typical products of the evolution of over-mature

organic matters [29]. Gas pores are widespread in the Longtan Formation shale from the Laochang area. The pores are nearly circular (Figure 1g) and irregularly distributed, and most are small in scale. The gas pore size was mostly smaller than 50 nm.

3.2.4. Fracture Pores

The rigid particles in the Longtan Formation shale from the Laochang area, such as feldspar and ankerite, are brittle, and they produce cleavages (Figure 1h) and fractures (Figure 1i) easily under stress, thereby improving pore connectivity. During the hydrocarbon generation and expulsion process, the organic matter shrunk continuously [30,31] and produced well-extended vein fractures. The shrinkage fractures in the organic matters and the rigid particle fractures are two types of fractures that were widely developed in the Longtan Formation shale in the study area.

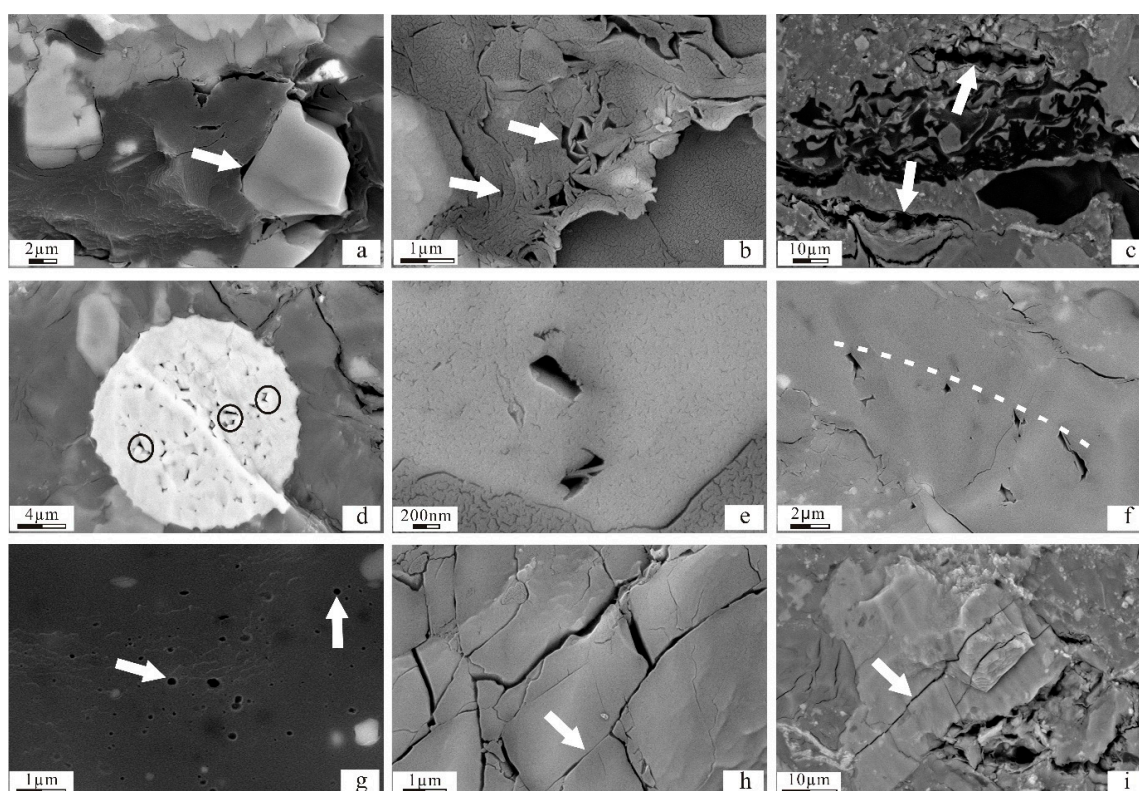


Figure 1. FE-SEM images of shale samples from the Laochang area, eastern Yunnan, China. (a) intergranular pores, at the margins of rigid partials and organic matter, S1 well, 746.8 m; (b) intergranular pores, between flexural deformed clay minerals, S2 well, 653.6 m; (c) dissolved pores, at the edge of particles, S2 well, 662.0 m; (d) intragranular pores, inside strawberry-like pyrite, S2 well, 662.0 m; (e) intragranular defect pores, within ankerite, S2 well, 653.6 m; (f) intragranular defect pores within ankerite distribute in band, S1 well, 823.7 m; (g) gas pores, inside the organic matter, S1 well, 789.2 m; (h) cleavage, inside the ankerite, S2 well, 653.6 m; and (i) fractures inside the feldspar, S2 well, 662.0 m.

3.3. Pore Morphology

A nitrogen isothermal adsorption-desorption curve can reflect the pore morphology and reveal the pore structure characteristics of a shale reservoir [32–35]. The overall shape of the adsorption curves of the Longtan Formation shale samples from the Laochang area resembles a reverse S-shape (Figure 2). When the relative pressure is low ($0 < P/P_0 < 0.3$), the mono-molecular layer transits to the multi-molecular layer during adsorption. The adsorption curve rises slowly, and the upward convex tendency is weak, indicating that the micropores are low in content. The middle part of the curve ($0.3 < P/P_0 < 0.8$) represents a multi-molecular layer adsorption process, and the adsorption amount

increases slowly with an increase in pressure, reflecting that the pores of the shale are dominated by mesopores. When the relative pressure is high ($0.8 < P/P_0 < 1.0$), the adsorption curve rises sharply, and no adsorption saturation occurs at the point where $P/P_0 = 1.0$, indicating that the samples contain some large pores and that adsorption aggregation occurs.

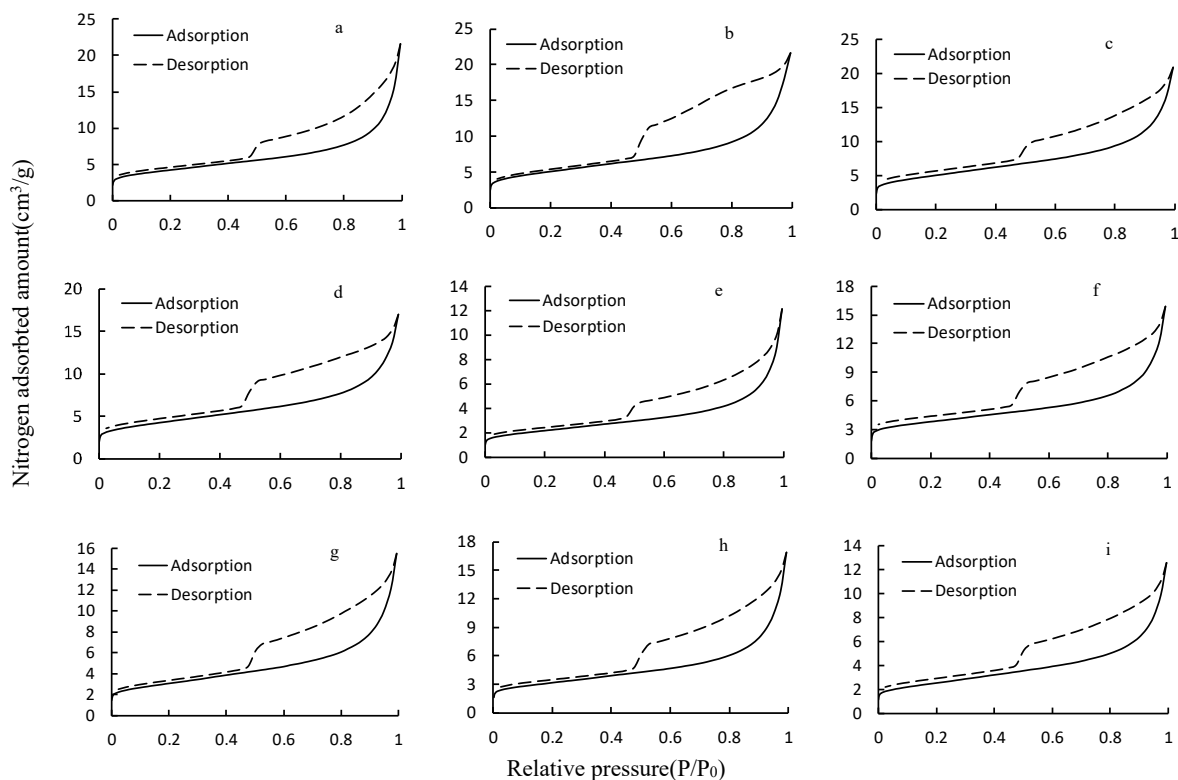


Figure 2. Low-temperature nitrogen adsorption and desorption isotherms. (a) S1 well, 746.8 m; (b) S1 well, 789.2 m; (c) S1 well, 823.7 m; (d) S2 well, 611.7 m; (e) S2 well, 632.03 m; (f) S2 well, 653.6 m; (g) S2 well, 662.0 m; (h) S2 well, 669.6 m; and (i) S2 well, 736.53 m.

The desorption curve is not consistent with the adsorption curve, resulting in a hysteresis loop. The adsorption curve is steep when the pressure is near the saturated vapor pressure, and the desorption curve appears steep at moderate pressure ($0.4 < P/P_0 < 0.6$) (Figure 2). The curves are similar to the Type B type return line recommended by DeBoer and the H3 type return line recommended by the International Union of Pure and Applied Chemistry (IUPAC), and have the characteristics of an H4 type return line, indicating that the pores of the shale are open and are dominated by the slit pores of the parallel wall and the cylindrical pores (including cylinders, cones, plates, etc.), containing only a small part of the irregular pores. At medium pressure ($0.4 < P/P_0 < 0.6$), the adsorption curves of the samples show a sharp drop inflection point, indicating that the samples contain a certain number of ink bottle pores, which are characterized by one end opening.

The openness degree and content of pores are related to the rising rate and the envelope range of the adsorption-desorption curve at higher pressure ($0.8 < P/P_0 < 1.0$). If the adsorption curve rises rapidly at a relatively high pressure, a greater openness degree is assumed. In addition, hysteresis indices, which are based on the areas under the adsorption and desorption isotherms, are used to quantitatively reflect the openness degree of the shale pores. A small hysteresis index represents a low openness degree of the shale pore [35–37]. As shown in Figure 2, it is assumed that in the S1 and S2 wells, with an increase in buried depth, the openness degree of the pores and the content of the open pores gradually decrease.

3.4. Pore Volume and Surface Area

The pore size and pore volume data obtained in the low temperature liquid nitrogen adsorption experiments (Table 2) show that the pore volume of the nine shale samples of the Longtan Formation from the Laochang area was generally 0.0157–0.0302 cm³/g, with an average of 0.0233 cm³/g. The pore diameter was 7.3–9.94 nm, with an average of 8.58 nm. The specific surface area was 7.578–17.307 m²/g, with an average value of 12.637 m²/g. The pore volume ratio of the micropores (V_1/V_t) was 6.1–9.4%, with an average of 7.7%. The pore volume ratio of the mesopores (V_2/V_t) was 77.2–82.2%, with an average of 79.9%. The pore volume ratio of the macropores (V_3/V_t) was 8.6–15.9%, with an average of 12.34%. It can be seen that the pore volumes and pore volume ratios of the mesopores are the largest, indicating that mesopores contribute the most to the shale reservoir space of the Longtan Formation. Compared with shale from the Longmaxi-Wufeng Formation in South Sichuan [21–25] and shale from the Shanxi-Taiyuan [26,27] and Yanchang Formations [28] in the Ordos basin, the pore structure of the Longtan Formation shale is characterized by a large average pore size, well-developed macropores, and high numbers of micropores and mesopores.

Table 2. Pore structure parameters of the shale samples from N₂ adsorption isotherms.

Sample ID	Depth (m)	S _{BET} (m ² /g)	AD (nm)	Volume (cm ³ /g)			V _{DFT} (mL/g)
				Micropore (<2 nm)	Mesopore (2–50 nm)	Macropore (>50 nm)	
S1-1	746.8	14.219	9.40	0.0023	0.0222	0.0042	0.0287
S1-2	789.2	17.261	7.78	0.0028	0.0248	0.0026	0.0302
S1-3	823.7	17.307	7.47	0.0025	0.0234	0.0028	0.0288
S2-1	611.7	14.443	7.30	0.0022	0.0188	0.0025	0.0235
S2-2	632.0	7.578	9.94	0.0010	0.0122	0.0025	0.0157
S2-3	653.6	12.696	7.74	0.0017	0.0167	0.0031	0.0215
S2-4	662.0	10.573	9.09	0.0013	0.0174	0.0025	0.0212
S2-5	669.6	10.789	9.71	0.0017	0.0181	0.0031	0.0229
S2-6	736.5	8.866	8.79	0.0010	0.0141	0.0020	0.0172

S_{BET}: BET surface area; V_{DFT}: total pore volume; AD: Average pore diameter.

4. Discussion

4.1. Factors Affecting the Distribution of Nanopores

4.1.1. Contribution of Organic Matter to Micropores and Mesopores

Organic matter pores have always been the research focus of shale pores and are the main factors affecting shale pores [38–40]. Organic matter pores generally show a tendency to increase with maturity [41]. Studies of shale pore evolution and main control factors show that the evolution of shale organic pores has multiple stages [42–44]. At the immature-mature stage ($R_o < 1.3\%$), the cells in the organic matter shrink and become plant tissue pores. Originating from the cell structure, plant tissue pores are large and regularly distributed in groups. At the high-over-mature stage ($1.3\% < R_o < 3.5\%$), a large amount of gaseous hydrocarbons composed of dry gas is generated. During this stage, gas pores, which are mainly round micropores and are irregular in distribution, are formed [29]. At the same time, the total volume of organic matter pores is maximized. The organic matter of the Longtan Formation shale from the Laochang area is type III, with an $R_o > 2.0\%$, which is typical of a high-over-mature shale (Table 1). The observations under argon ion polishing field emission scanning electron microscopy show that gas pores are widespread in the organic matter of the Longtan Formation shale in the study area (Figure 1g). These gas pores are large in number and small in size. With a pore diameter of 50 nm, they belong to micropores and mesopores. The organic carbon content of the Longtan Formation shale has a positive correlation with the micropores and mesopores (correlation coefficients of 0.61 and 0.63),

and a certain correlation with the macropores (correlation coefficient of 0.33) (Figure 3). The above facts indicate that in the high-over-mature shale of the Longtan Formation from the Laochang area, gas pores are the main organic pore types and are the important pore type that constitutes micropores and mesopores in shale reservoirs. In addition, organic pores also contribute to macropores to some extent.

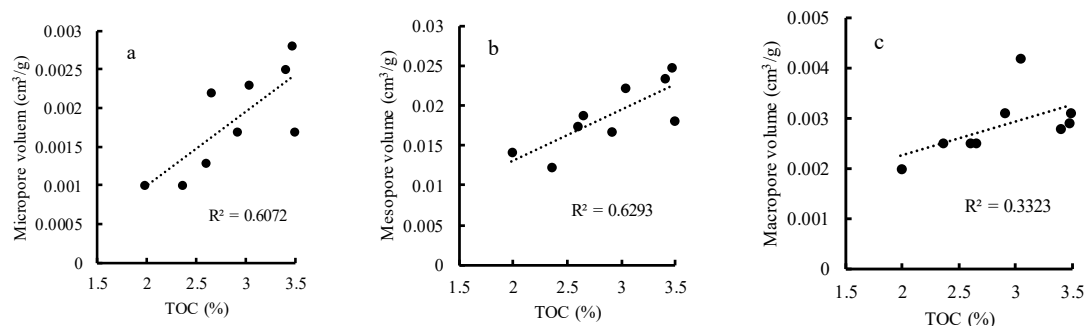


Figure 3. (a) The relationship between Micropore volume and TOC. (b) The relationship between Mesopore volume and TOC. (c) The relationship between Macropore volume and TOC.

4.1.2. Contribution of Clay Minerals to Micropores and Mesopores

X-ray diffraction tests show that the high-over-mature shale of the Longtan Formation is rich in clay minerals (Table 1), which can provide inter-clay pores. Through scanning electron microscopy, the clay minerals were observed to have an obvious orientation and formed widespread inter-clay pores. The pore diameter of the inter-clay pores is less than 50 nm, and 15 nm on average (Figure 1b), which belongs to micropores and mesopores. The nitrogen adsorption-desorption curve show that the pores of the Longtan Formation shale are open and are dominated by parallel narrow pores and cylinder pores with two open ends (Figure 2), which is consistent with the observation results from the scanning electron microscopy. The mineral composition of the shale and the results of the nitrogen adsorption test match well. The micropores and mesopores of the Longtan Formation shale from the Laochang area were found to have a strong positive correlation with the clay mineral content (correlation coefficients of 0.66 and 0.79), while the macropores are not related to the clay minerals (Figure 4). From the above, it is concluded that the micropores and mesopores of the Longtan Formation shale from the Laochang area are dominated by inter-clay pores.

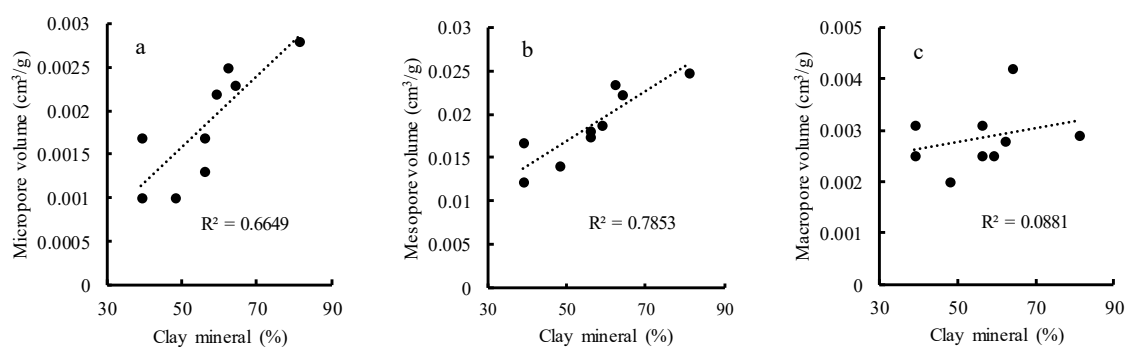


Figure 4. (a) The relationship between micropore volume and clay mineral content. (b) The relationship between mesopore volume and clay mineral content. (c) The relationship between macropore volume and clay mineral content.

4.2. Contribution of Dissolved Pores to Macropores

Through observation with scanning electron microscopy, dissolved pores were found to generally develop in the area adjacent to organic matter (Figure 1c). These dissolved pores constituted the macropores of the shale together with the intergranular pores and micro-fractures. According to the classification scheme of shale micropores [45–47], it can be concluded that the development of

intergranular pores and micro-fractures has a direct relationship with brittle minerals, while the formation and development of dissolved pores are related to many factors, such as the carbonate minerals and feldspar in organic matters and brittle minerals. The organic matter of the Longtan Formation shale has a type III kerogen, and is at the high-over-mature stage. A large amount of organic acids was generated during the early hydrocarbon generation. These organic acids acted on the acid-resistant minerals. As a result, a large number of dissolved pores were formed. It can be seen from Figure 5 that the macropore volume of high-over-mature shales has no relationship with the brittle minerals content, but it has a small positive correlation with the plagioclase content (correlation coefficient of 0.25), indicating that intergranular pores and micro-fractures are not the main part of macropores. The dissolved pores formed by the dissolution of the plagioclase provide a large number of macropores to the high-over-mature shale of the Longtan Formation.

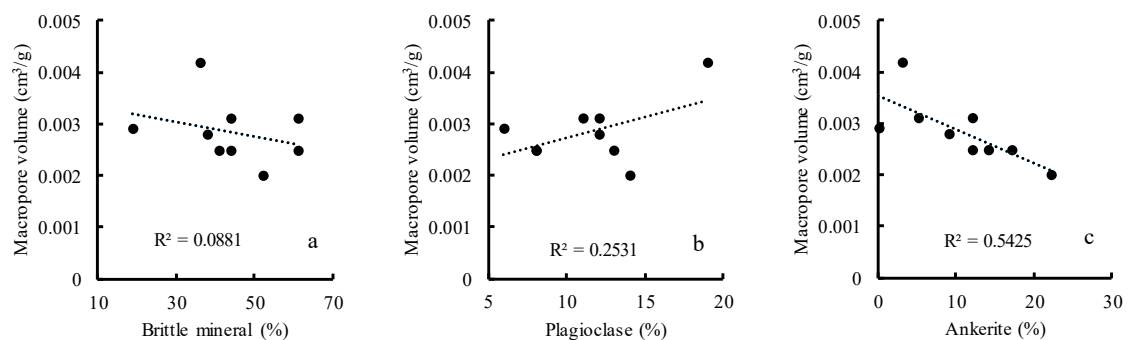


Figure 5. (a) The relationship between macropore volume and brittle minerals content. (b) The relationship between macropore volume and plagioclase content. (c) The relationship between macropore volume and ankerite content.

4.3. Impact of Ankerite on Shale Pores

The organic matter of the Longtan Formation shale has reached a high-over-mature stage, and gaseous hydrocarbons dominated by dry gas is generated in large quantities at this stage. At the same time, diagenesis enters the late diagenetic stage B, and carbonate metasomatism is widely developed. Basalt eruption and basic magma intrusions in the Late Permian [17] provided a large number of ferrous ions for the metasomatism of ankerite at the late diagenetic stage. Affected by a large number of gaseous hydrocarbons, the newly formed ankerite generally develops intragranular defect macropores (Figure 1e,f). In addition, the newly formed ankerite provides macro-cleavage fractures (Figure 1h) and rigid intergranular pores (Figure 1e) for the shale. However, compared with the occlusion of newly formed ankerite in the shale, these macropores related to the formation of ankerite have not contributed enough to the pore structure of the shale. There is a strong negative correlation between the ankerite content and the macropore volume in the Longtan Formation shale in the study area (Figure 5) (correlation coefficient of 0.54). This relationship indicates that the ankerite in high-over-mature shale is the main destroyer of the pores in shale, especially macropores.

4.4. Oil and Gas Geological Significance

In the Laochang area, basalt eruptions and basic magma intrusions occurred in the Late Permian [17]. The Longtan Formation had a maximum buried depth of more than 4000 m due to the intense tectonic subsidence at the end of the Indosinian period [20]. Under the joint action of rock mass emplacement and deep burial, the organic matter of the Longtan Formation shale reached the high-over-mature stage and the diagenesis of the shale entered the late diagenetic stage B. During this stage, the internal components of the shale were transformed coordinatively, and the special pore structure in the over-mature shale was formed. Organic matter discharged acids at the early hydrocarbon generation stage, and the acids acted on acid-resistant minerals, such as feldspar and calcite, forming a large number of dissolved pores with large pore diameters (greater than 1000

nm). A large number of pores with small pore diameters (less than 50 nm) formed as a result of the hydrocarbon expulsion from the high-over-mature organic matter at the late stage. At the same time, they shrank and formed micro-fractures. Clay minerals were transformed and oriented to form a large number of inter-clay pores with small pore sizes (less than 50 nm). A large amount of ankerite formed due to the metasomatism at the late diagenetic stage, causing some shale pores to become occluded. However, intragranular pores and cleavage fractures with large pore diameters developed inside the ankerite, which contributed to some macropores in the shale reservoirs. It can be seen that the evolution of high-over-mature shale reservoirs was a gradual adjustment process concerning their internal composition and structure. Comprehensive analyses of the disappearance of pores and the formation of new pores in this process are particularly important for improving the accuracy of shale reservoir evaluations.

5. Conclusions

- (1) With an average Ro value of 2.29%, the Longtan Formation shale is a typical over-mature shale. The average pore diameter was 8.58 nm, which is at the nanopore scale. The average value of the specific surface area was 12.637 m²/g, while the average value of the total pore volume was 0.0233 cm³/g. The average pore volume ratios of micropores, mesopores, and macropores were 7.74%, 79.9%, and 12.34%, respectively.
- (2) The clay minerals in the over-mature shale were oriented, and gas pores were widespread in organic matters. The inter-clay pores and organic matter pores constituted the main part of the micro and mesopores of the shale, between which the contribution of inter-clay pores was slightly larger than that of organic matter pores.
- (3) The constitution and formation of macropores in high-over-mature shale is complex and is a comprehensive product of the coordinated evolution of the internal components of shale. During the formation of high-over-mature shale, intense compaction results in the massive destruction of intergranular pores (mainly macropores) and the formation of some micro-fractures in rigid minerals. The dissolution of non-acid-resistant minerals by organic acids forms a large number of dissolved pores with large pore sizes. The thermal evolution of high-over-mature organic matter forms part of macropores and shrinkage fractures of organic matter. The macropores of the Longtan Formation shale in the Laochang area consisted of dissolved pores, gas pores, the intergranular pores of residual rigid minerals, and micro-fractures.
- (4) Hydrocarbon expulsion and carbonate metasomatism occur simultaneously in high-over-mature shale at the late stage. The Late Permian basalt eruption and basic magma provided sufficient ferrous ion. At the late diagenetic stage B, a large amount of the ankerite formed by metasomatism occluded some macropores of the shale. However, ankerite crystallized under the action of gaseous hydrocarbons and intragranular pores formed inside. These intragranular pores, together with the cleavage fractures inside ankerite, provided a small amount of macropores for the shale reservoir, which is beneficial to the improvement of reservoir quality.

Author Contributions: Writing—Original Draft Preparation, X.Z. and J.H.; Writing—Review & Editing, C.W.; Experiments & Data Processing, Z.R. and T.Z.

Funding: This study was supported by the National Natural Science Foundation of China (No. 41702170) and a Project Funded by the Priority Academic Program Development of Jiangsu Higher Education Institutions.

Conflicts of Interest: The authors declare no conflict of interest.

References

1. Zou, C.; Dong, D.; Wang, S.; Li, J.; Li, X.; Wang, Y.; Li, D.; Cheng, K. Geological characteristics, formation mechanism and resource potential of shale gas in China. *Pet. Explor. Dev.* **2010**, *37*, 641–653. [[CrossRef](#)]
2. Manger, K.C.; Oliver, S.J.P.; Curtis, J.B.; Scheper, R.J. *Geologic Influences on the Location and Production of Antrim Shale Gas, Michigan Basin*. SPE 21854; Society of Petroleum Engineers: Denver, CO, USA, 1991.

3. Curtis, J.B.; Faure, G. Accumulation of organic matter in the in the Rome trough of the Appalachian basin and its subsequent thermal history. *AAPG Bull.* **1997**, *81*, 424–437.
4. Montgomery, S.L.; Jarvie, D.M.; Bowker, K.A.; Pollastro, R.M. Mississippian Barnett Shale, Fort Worth Basin, north-central Texas: Gas-shale play with multi-trillion cubic foot potential. *AAPG Bull.* **2005**, *89*, 155–175. [[CrossRef](#)]
5. Hammes, U.; Hamlin, H.S.; Ewing, T.E. Geologic Analysis of the Upper Jurassic Haynesville shale in east Texas and west Louisiana. *AAPG Bull.* **2011**, *95*, 1643–1666. [[CrossRef](#)]
6. Chalmers, R.G.; Bustin, R.M.; Power, M.I. Characterization of Gas shale pore systems by porosimetry, pycnometry, surface area and field emission scanning electron microscopy/transmission electron microscopy image analyses: Examples from the Barnett, Woodford, Haynesville, Marcellus, and Doig Units. *AAPG Bull.* **2012**, *96*, 1099–1119. [[CrossRef](#)]
7. Zhang, J.; Xu, B.; Nie, H.; Wang, Z.; Lin, T.; Jiang, S.; Song, X.; Zhang, Q.; Wang, G.; Zhang, P. Exploration potential of shale gas resources in China. *Nat. Gas Ind.* **2008**, *6*, 136–140, 159–160.
8. Nie, H.; Tang, X.; Bian, R. Controlling factors for shale gas accumulation and prediction of potential development area in shale gas reservoir of South China. *Acta Pet. Sin.* **2009**, *30*, 484–491.
9. Cao, T.; Song, Z.; Wang, S.; Xia, J. A comparative study of the specific surface area and pore structure of different shales and their kerogens. *Sci. China Earth Sci.* **2015**, *45*, 139–151. [[CrossRef](#)]
10. Li, J.; Dong, D.; Chen, G.; Wang, S.; Cheng, K. Prospects and strategic position of shale gas resources in China. *Nat. Gas Ind.* **2009**, *29*, 112–116.
11. Zou, C.; Yang, Z.; Tao, S.; Li, W.; Wu, S.; Hou, L.; Zhu, R.; Yuan, X.; Wang, L.; Gao, X.; et al. Nano-hydrocarbon and the accumulation in coexisting source and reservoir. *Pet. Explor. Dev.* **2012**, *39*, 13–26. [[CrossRef](#)]
12. Jia, C.; Zheng, M.; Zhang, Y. Unconventional hydrocarbon Resources in China and the prospect of exploration and development. *Pet. Explor. Dev.* **2012**, *39*, 129–136. [[CrossRef](#)]
13. Dong, D.; Wang, Y.; Li, X.; Zou, C.; Guan, Q.; Zhang, C.; Huang, J.; Wang, S.; Wang, H.; Liu, H.; et al. Breakthrough and prospect of shale gas exploration and development in China. *Nat. Gas Ind.* **2016**, *36*, 19–32. [[CrossRef](#)]
14. Durand, B.; Nicaise, G. Procedures for Kerogen Isolation. In *Kerogen-Insoluble Organic Matter from Sedimentary Rocks*; Durand, B., Ed.; Technip: Paris, France, 1980; pp. 35–53.
15. Fu, J.; Wang, B.; Shi, J.; Jia, R.; Sheng, G. Evolution of organic matter and origin of sedimentary ore deposits. *Acta Sedimentol. Sin.* **1983**, *1*, 41–58.
16. Yu, B. Particularity of shale gas reservoir and its evaluation. *Earth Sci. Front.* **2012**, *19*, 252–258.
17. Yuan, Y.; Chen, W.; Cao, Y. Sedimentary Environment and Coal Accumulation of the Third Member, Longtan Formation, Laochang Mining Field, Fuyuan County, Yunnan Province. *Guizhou Geol.* **2008**, *3*, 171–176.
18. Li, W.; Zhu, Y.; Chen, S.; Wang, M.; Wang, H.; Zhong, H. Multilayer Superimposed CBM-bearing Independent System in Laochang Mine Area, Eastern Yunnan. *Coal Geol. China* **2010**, *22*, 18–21.
19. Wu, C.; Wang, X.; Liu, X.; Zhou, H. Study on geostress features and influences under multi-seam condition in Laochang Mining Area of East Yunnan. *Coal Sci. Technol.* **2019**, *47*, 118–124.
20. Zhu, Y.; Zhao, H.; Yan, Q.; Wang, H.; Fang, J. Tectonic Evolution and CBM Reservoir Formation in Wulunshan Minefield, Guizhou. *Coal Geol. China* **2008**, *10*, 38–41.
21. Zhang, S.; Meng, Z.; Guo, Z.; Zhang, M.; Han, C. Characteristics and major controlling factors of shale reservoirs in the Longmaxi Formation, Fuling area, Sichuan Basin. *Nat. Gas Ind.* **2014**, *34*, 16–24.
22. Wang, Y.; Dong, D.; Yang, H.; He, L.; Wang, S.; Huang, J.; Pu, B.; Wang, S. Quantitative characterization of reservoir space in the Lower Silurian Longmaxi Shale, southern Sichuan, China. *Sci. China Earth Sci.* **2014**, *57*, 313–322. [[CrossRef](#)]
23. Jin, Z.; Hu, Z.; Gao, B.; Zhao, J. Controlling factors on the enrichment and high productivity of shale gas in the Wufeng-Longmaxi Formation, southeastern Sichuan Basin. *Earth Sci. Front.* **2016**, *23*, 1–10.
24. Wang, P.; Li, C.; Zhang, L.; Zou, C.; Li, X.; Wang, G.; Jiang, L.; Zhang, C.; Li, J.; Mei, Y. Characteristic of the shale gas reservoirs and evaluation of sweet spot in Wufeng—Longmaxi Formation: A case from the A well in Zhaotong shale gas demonstration zone. *J. China Coal Soc.* **2017**, *42*, 2925–2935.
25. Tang, X.; Zhu, Y.; Guo, Y.; Liu, Y.; Zhou, X. Molecular simulation of methane adsorption within illite minerals in the shale of the Longmaxi Formation based on a grand canonical monte carlo method and pore size distribution. *Nat. Gas Geosci.* **2018**, *29*, 1809–1816. [[CrossRef](#)]
26. Sun, C.; Tang, S.; Wei, J. The differences of reservoir feature between southern marine shale gas and northern coal-bearing shale gas in China. *China Min. Mag.* **2017**, *26*, 166–170.

27. Wen, F.; Zhu, Y.; Ren, Z.; Ni, J.; Gao, P. Reservoir porosity characteristics and controls of the Shanxi Formation shale reservoir, Yanchang area, Ordos Basin. *Pet. Geol. Exp.* **2018**, *40*, 778–785.
28. Sun, B.; Zhang, T. Reservoir characteristics and its influence of Chang 7 lacustrine shale, Zhangjiawan area, Ordos basin. *Nat. Gas Geosci.* **2019**, *30*, 274–284.
29. Chen, Y.; Qin, Y.; Wei, C.; Huang, L.; Shi, Q.; Wu, C.; Zhang, X. Porosity changes in progressively pulverized anthracite subsamples: Implications for the study of closed pore distribution in coals. *Fuel* **2018**, *225*, 612–622. [[CrossRef](#)]
30. Sondergeld, C.H.; Rai, C.S.; Curtis, M.E. Relationship between Organic Shale Microstructure and Hydrocarbon Generation. In Proceedings of the SPE Unconventional Resources Conference–USA, The Woodlands, TX, USA, 10–12 April 2013.
31. Loucks, R.G.; Reed, R.M. Scanning-electron-microscope petrographic evidence for distinguishing organic-matter pores associated with depositional organic matter versus migrated organic matter in mudrock. *Gulf Coast Assoc. Geol. Soc.* **2014**, *3*, 51–60.
32. Deboire, J.H. The Shape of Capillaries. In *The Structure and Properties of Porous Materials*; Everett, D.H., Stone, F.S., Eds.; Butterworth: London, UK, 1958.
33. Yan, J.; Zhang, Q. *Adsorption and Condensation*; Science Press: Beijing, China, 1979.
34. Zhao, Z.; Tang, X. Study of micropore in coal by low temperature nitrogen adsorption method and its significance. *Coal Geol. Explor.* **2001**, *29*, 28–30.
35. Chen, S.; Zhu, Y.; Wang, H.; Liu, H.; Wei, W.; Fang, J. Structure characteristics and accumulation significance of nanopores in Longmaxi shale gas reservoir in the southern Sichuan Basin. *J. China Coal Soc.* **2012**, *37*, 438–444.
36. Zhu, H.; Selim, H.M. Hysteretic behavior of metolachlor adsorption-desorption in soils. *Soil Sci.* **2000**, *165*, 632–645. [[CrossRef](#)]
37. Wang, K.; Wang, G.; Ren, T.; Cheng, Y. Methane and CO₂ sorption hysteresis on coal: A critical review. *Int. J. Coal Geol.* **2014**, *132*, 60–80. [[CrossRef](#)]
38. Curtis, M.E.; Cardott, B.J.; Sondergeld, C.H.; Rai, C.S. Development of organic porosity in the woodford shale with increasing thermal maturity. *Int. J. Coal Geol.* **2012**, *103*, 26–31. [[CrossRef](#)]
39. Yang, Y.; Wu, K.; Zhang, T.; Xue, M. Characterization of the pore system in an over-mature marine shale Reservoir: A case study of a successful shale gas well in southern Sichuan Basin, China. *Petroleum* **2015**, *1*, 173–186. [[CrossRef](#)]
40. He, R.; Jia, W.; Peng, P. Influence of hydrocarbon expulsion and retention on the evolution of nanometer-scale pores in organic matter rich shale: An example from pyrolysis experiment. *Geochimica* **2018**, *5*, 575–585.
41. Jarvie, D.M.; Hill, R.J.; Ruble, T.E.; Pollastro, R.M. Unconventional shale-gas systems: The mississippian barnett shale of north-central texas as one model for thermogenic shale-gas assessment. *AAPG Bull.* **2007**, *91*, 475–499. [[CrossRef](#)]
42. Mastalerz, M.; Schimmelmann, A.; Drobnia, A.; Chen, Y.Y. Porosity of Devonian and Mississippian New Albany Shale across a maturation gradient: Insights from organic petrology, gas adsorption, and mercury intrusion. *AAPG Bull.* **2013**, *97*, 1621–1643. [[CrossRef](#)]
43. Milliken, K.L.; Rudnicki, M.; Awwiller, D.N.; Zhang, T.W. Organic matter-hosted pore system, Marcellus Formation (Devonian), Pennsylvania. *AAPG Bull.* **2013**, *97*, 177–200. [[CrossRef](#)]
44. Klaver, J.; Desbois, G.; Littke, R.; Urai, J.L. BIB-SEM characterization of pore space morphology and distribution in postmature to overmature samples from the Haynesville and Bossier Shales. *Mar. Pet. Geol.* **2015**, *59*, 451–466. [[CrossRef](#)]
45. Slatt, E.M.; O’Neal, N.R. Pore types in the Barnett and Wood-ford Gas shales: Contribution to Understanding Gas storage and migration pathways in fine-grained Rocks. *AAPG Bull.* **2011**, *95*, 2017–2030. [[CrossRef](#)]
46. Loucks, R.G.; Reed, R.M.; Ruppel, S.C.; Hammes, U. Spectrum of pore types and networks in mudrocks and a descriptive classification for matrix-related mudrock pores. *AAPG Bull.* **2012**, *96*, 1071–1098. [[CrossRef](#)]
47. Yu, B. Classification and characterization of gas shale pore system. *Earth Sci. Front.* **2013**, *20*, 211–220.

